Sticholysin I–membrane interaction: An interplay between the presence of sphingomyelin and membrane fluidity

Lohans Pedrera [a], Maria Laura Fanani [b,*], Uris Ros [a], María E. Lanio [a], Bruno Maggio [b], Carlos Álvarez [a,**]

[a] Centro de Estudio de Proteínas, Facultad de Biología, Universidad de la Habana, CP 10400 La Habana, Cuba
[b] Departamento de Química Biológica, Centro de Investigaciones en Química Biológica de Córdoba (CIQUIBIC), Facultad de Ciencias Químicas-CONICET, Universidad Nacional de Córdoba, X5000HUA Córdoba, Argentina

ABSTRACT

Sticholysin I (St I) is a pore-forming toxin (PFT) produced by the Caribbean Sea anemone *Stichodactyla helianthus* belonging to the actinoporin protein family, a unique class of eukaryotic PFT exclusively found in sea anemones. As for actinoporins, it has been proposed that the presence of sphingomyelin (SM) and the coexistence of lipid phases increase binding to the target membrane. However, little is known about the role of membrane structure and dynamics (phase state, fluidity, presence of lipid domains) on actinoporins' activity or which regions of the membrane are the most favorable platforms for protein insertion. To gain insight into the role of SM on the interaction of St I to lipid membranes we studied their binding to monolayers of phosphatidylcholine (PC) and SM in different proportions. Additionally, the effect of acyl chain length and unsaturation, two features related to membrane fluidity, was evaluated on St I binding to monolayers. This study revealed that St I binds and penetrates preferentially and with a faster kinetic to liquid-expanded films with high lateral mobility and moderately enriched in SM. A high content of SM induces a lower lateral diffusion and/or liquid-condensed phases, which hinder St I binding and penetration to the lipid monolayer. Furthermore, the presence of lipid domain borders does not appear as an important factor for St I binding to the lipid monolayer.

© 2014 Published by Elsevier B.V.

1. Introduction

Pore forming toxins (PFTs) play an active role in the defense systems of different kingdoms of life [1,2]. Besides its biological relevance, pore formation in lipid membrane by PFT has received special attention as model systems to understand basic molecular mechanism of protein insertion into membranes. Actinoporins are highly basic proteins, of a single polypeptide chain, with molecular weight around 20 kDa exclusively produced by sea anemones whose putative receptor is SM [2,3].

They are classified as α-PFT because their mechanism of pore formation involves the insertion of the N-terminal α-helix in the membrane [4,5]. St I is an actinoporin of 176 amino acid residues purified from the Caribbean Sea anemone *Stichodactyla helianthus* which displays a hemolytic activity at rather low concentrations [6].

The mechanism of pore formation proposed for actinoporins is based on an initial binding step followed by oligomerization and membrane insertion leading to pore formation [7]. For actinoporins, it has been proposed that binding to membranes is favored both by the presence of SM [3,8–13] and/or the coexistence of lipid phases [14–17]. However, the role of membrane structure and dynamics on actinoporins' initial binding or which regions of membrane are the most favorable platforms for protein recognition are not well understood. In fact, based on indirect evidence it was proposed that lipid packing defects arising at the interface between coexisting lipid phases may function as preferential binding sites for equinatoxin II (Eqt II), an actinoporin from *Actinia equina* [14]. However, there is no robust experimental data regarding the preferential membrane localization of sticholysins or in a more general sense it has not been described how the lipid molecular packing or acyl chain alignment affects the initial binding of actinoporins to membranes. In particular, the influence of phospholipid acyl chain length and unsaturation, two features related to membrane fluidity, have not been systematically studied in the effect of the actinoporin family.

In the present study, we used lipid monolayers as a model membrane to study the first step of St I binding to membrane. The combination of monolayer compression isotherms, Brewster angle microscopy (BAM) and fluorescence recovery after photobleaching (FRAP) experiments provided detailed information on the structural and rheological properties of the monolayers and allow correlating them with the affinity of St I for lipid films. Additionally, fluorescence microscopy (FM) imaging revealed the preferential localization of St I in different lipid phases. These results provided further insight into the initial binding and recognition of St I to lipid membrane, and reveal that the toxin association to model membranes is a result of a subtle interplay between the presence of SM and membrane fluidity.

2. Materials and methods

2.1. Chemicals and reagents

St I was purified from the sea anemone *S. helianthus* by combining gel filtration chromatography on Sephadex G-50 medium (Pharmacia-LKB, Sweden) and cationic exchange chromatography on CM-cellulose 52 (Whatman, Maidstone, UK) as previously described [6]. Lipids were from Avanti Polar Lipids (Alabaster, AL) and used without further purification. The lipophilic fluorescent probes Rho-PE and NBD-DPPE, and the amine-reactive probe Alexa Fluor 488 carboxylic acid succinimidyl ester were purchased from Invitrogen (Eugene, OR). Solvents and chemicals were of the highest commercial purity available. Water was purified by a Milli-Q system (Millipore, Billerica, MA), to yield a product with a resistivity of ~18.5 M$\Omega \cdot$cm^{-1}. The absence of surface-active impurities was routinely checked as described elsewhere [18].

2.2. Binding of St I to lipid monolayers

Surface pressure (π) measurements were carried out with a μTrough-S system (Kibron, Helsinki, Finland) at 23 ± 2 °C under constant stirring. The subphase consisted of 300 μL of Tris-buffered saline (TBS: 145 mM NaCl, 10 mM Tris–HCl, pH 7.4). Lipid monolayers were formed by spreading a lipid chloroformic solution over the surface to attain an initial surface pressure (π_0) of ~20 mN$\cdot$m^{-1}. After 5 min for allowing solvent evaporation, St I was injected into the subphase to achieve 0.8 μM protein final concentration. Similar to St II [17], at this subphase concentration St I has no effect on surface tension of the air–buffer interface. The increment in surface pressure ($\Delta\pi$) was recorded as a function of time until a stable signal was obtained. The initial maximal rate (V_0) was evaluated within the first 10 s of toxin penetration experiments, where a linear relationship of π with time was observed.

2.3. Monolayer compression isotherms

Compression isotherms were obtained for pure or mixed lipid monolayers by spreading 25 μL of a chloroformic solution onto a Teflon through filled with 145 mM NaCl, pH 5.6. The film was relaxed for 5 min at 0 mN$\cdot$m^{-1} and subsequently compressed at a rate of 1 Å$^2\cdot$molecule$^{-1}\cdot$min^{-1} to the collapse pressure. π and the film area were continuously measured and recorded with a KSV Minitrough equipment (KSV, Helsinki, Finland). The phase transition points were estimated by the third derivate method [19]. In order to compare the phase state and the rheology properties of the film, the compressibility modulus (Cs^{-1}) was calculated at 20 mN$\cdot$m^{-1} from the isotherm data as [19]:

$$Cs^{-1} = -MMA\left(\frac{\partial\pi}{\partial MMA}\right)_T \tag{1}$$

where *MMA* is the mean molecular area of the lipid monolayer at 20 mN$\cdot$m^{-1} at a constant temperature (*T*).

2.4. Brewster angle microscopy of lipid monolayers

The monolayers were observed while compressed using BAM. A KSV Minitrough equipment (KSV, Helsinki, Finland) was placed on the stage of an autonulling Nanofilm EP3 Imaging Elipsometer (Accurion, Gottingen, Germany) used in the BAM mode. Zero reflection was set with a polarized laser ($\lambda = 532$ nm) incident on the bare aqueous surface at the experimentally calibrated Brewster angle ($\approx 53.1°$). After monolayer formation and compression, the reflected light was collected with a 20× objective.

2.5. Fluorescence recovery after photobleaching assay

FRAP experiments were performed using a confocal Olympus FV1000 microscope equipped with a CCD camera. The lipid mixture containing the fluorescent probe NBD-DPPE (1 mol%) was spread over a surface of TBS, until reaching a π_0 of ~20 mN$\cdot$m^{-1}. Afterwards, the subphase level was reduced to ~1 mm thickness to minimize convection. Before bleaching, a stack of five images was scanned to record the pre-bleach fluorescence. The bleaching spot was set by a circular region of 20 μm diameter illuminated at maximal potential for 15 s using a 20× objective. The fluorescence recovery was recorded in a series of images with a temporal spacing of 1.2 s. In order to characterize the lateral diffusion of the lipid in the monolayers we calculated the $t_{3/4}$ parameter which is the time at 75% recovery, by fitting the normalized fluorescence ($f_{(t)}/f_{(0)}$) *vs* time (*t*) to the single exponential function:

$$\left(f_{(t)}/f_{(0)}\right) = a - bc^t \tag{2}$$

where *a*, *b*, and *c* are the fitting coefficients of the exponential.

2.6. Conjugation of St I with Alexa dye

Conjugation of St I with the dye was performed in 100 mM NaHCO$_3$ (pH 8.3) buffer. St I was incubated with the amine-reactive dye Alexa Fluor 488 carboxylic acid succinimidyl ester, which was dissolved in dimethylsulfoxide and immediately added to the protein solution. The final dimethylsulfoxide dilution in the examined sample was 1:10. The reaction mixture was incubated for 1 h in the dark at room temperature under constant stirring. The conjugated protein was separated from the unreacted dye by filtering through Amicom Ultra 0.5 10 K filter (Millipore Corp., USA). The obtained conjugate had an average ratio of 2:1 Alexa/St I (calculated from absorbance measurements). The Alexa-St I conjugate was 1:5 diluted with unlabeled toxin and stored in the dark at 4 °C until use. The activity of the toxin mixture was similar to the unlabeled toxin as demonstrated by a hemolytic assay described elsewhere [20].

2.7. Visualization of St I-Alexa conjugate bound to supported monolayers

A combined Langmuir–Blodgett/Langmuir–Schaefer technique was used to visualize Alexa-St I insertion to lipid monolayers [21,22]. A first Langmuir–Blodgett transference of DPPC monolayer (at 30 mN$\cdot$m^{-1}) to clean glass coverslips was performed in a KSV Minitrough equipment (KSV, Helsinki, Finland) with the aim of obtaining an hydrophobic surface: after DPPC monolayer formation the film was transferred to the glass coverslips by moving it vertically upwards at a rate of 3 mm$\cdot$min^{-1}, and keeping automatically a constant π. Then, a second lipid monolayer was added by the Langmuir Schaefer method as previously described [22]. Briefly, after forming the lipid-Rho-PE (1 mol%) film at a π_0 of 20 mN$\cdot$m^{-1} in a 1 mL circular compartment of a μThrough-S equipment (Kibron, Helsinki, Finland) the 1:5 mixture of Alexa-St I/unlabeled St I was injected into the subphase to reach a final concentration of 0.8 μM. When a stable π signal was obtained, the hydrophobic coverslip was lowered horizontally until touching the film. The

coverslip was pushed through the monolayer and gently washed before being observed through the microscope.

Fluorescence visualization of the St I-loaded (second) transferred monolayer was carried out on a Zeiss Axioplan microscopy (Carl Zeiss, Oberkochen, Germany) using a mercury lamp (HBO 50), a 63× water-LD objective and a CCD Olympus MX10 camera (Olympus Corp. USA). The images were taken using the acquisition software without activating the auto-contrast mode in order to keep a quantitative Alexa labeled-St I–gray level relationship. Background fluorescence was subtracted from control experiments. The partition ratio of labeled-St I to the liquid-condensed (Lc) and liquid-expanded (Le) phases in heterogeneous monolayers was calculated from the ratio of gray level in the two coexistent phases in each picture. The error caused by quenching of the film fluorescence was eliminated by calculating the Le/Lc fluorescence ratio for each image independently, and considering that the fluorescence quenching would affect equally both phases. At least ten measurements accomplished in two independent samples were imaged for each monolayer composition. All the experiments were carried out at 23 ± 2 °C.

2.8. Estimation of the mole fraction of each lipid component in the Le and Lc lipid phases

In order to analyze the St I's preferential binding to lipid monolayers showing phase coexistence we performed studies to estimate the lipid composition of each lipid phase. To this purpose, we prepared binary lipid monolayers in different proportions and visualized them by BAM. In all cases the increase of the proportion of the lipids containing saturated acyl chains induced a progressive rise of the area occupied by the Lc phase. From the experimental data of MMA of the pure lipids in Le and Lc phases, derived from their compression isotherms, and the proportion of area occupied by each phase in the same mixed monolayers (calculated by using the free software ImageJ, NIH USA), the composition of each coexisting phase was estimated considering that they belong to the same tie-line, as follows [23]:

$$\frac{A^{\mathrm{Le}}}{A^{\mathrm{Lc}}} = \frac{MMA^{\mathrm{Le}}}{MMA^{\mathrm{Lc}}} \frac{X^{\mathrm{Lc}} - X}{X - X^{\mathrm{Le}}} \qquad (3)$$

where A^{Le} and A^{Lc} are the fractional area occupied by the Le and Lc lipid phases from the total area of the monolayer. MMA^{Le}, MMA^{Lc} are the mean molecular area of the lipids in the Le or Lc phase and, X^{Le}, X^{Lc} are the mole fraction of the most condensed lipid in the mixed monolayer, in the Le and Lc phases, respectively.

2.9. Statistical analysis

Statistical analysis was performed using SPSS software version 16.0 (IBM SPSS Statistics, Madrid, Spain). The Kolmogorov–Smirnov test was used to verify normal distribution of data and the Levene test to determine the homogeneity of variance. Data with normal distribution and homogeneity of variance were analyzed with the one-way variance analysis (ANOVA) simple classification and Tukey as post-hoc test to assess statistical significance between the means of independent groups (namely a, b, c… in each figure and table).

3. Results and discussion

3.1. Interaction of St I with PC:eSM monolayers

Several actinoporin family members have shown preferences for binding to SM-enriched membranes [3,8–14]. In order to gain insight into the influence of SM content on St I interaction with membranes, we prepared lipid monolayers over a broad range of POPC/eSM proportions. The injection of St I (0.8 μM) into the subphase of the monolayers at 20 mN·m^{-1} triggered an increase in π (Δπ) which became stabilized

after ~300 s (Fig. 1A). The Δπ elicited by the association of the toxin to a previously formed lipid monolayer can be employed to characterize the ability of the toxin to interact with organized lipids [24]. Binding of St I to lipid monolayer was maximum at POPC/eSM equimolar proportions and diminished significantly when one of the two phospholipids predominated (Fig. 1B). Also, a similar effect was detected for the rate of St I insertion into the film showing a maximum in the equimolar mixture (Fig. 1C).

This result is in clear correspondence to previous reports regarding the higher affinity of St I [3] and St II [17], for bilayers and monolayers respectively, when the lipidic mixture contains equal molar proportions of PC and SM. In fact, this behavior seems to be common for actinoporins as already observed for Eqt II [14] and fragaceatoxin C, a related actinoporin from *Actinia fragacea* [13]. Based on evidence obtained in lipid bilayers describing the liquid crystalline/gel phase coexistence at equimolar proportion of PC/SM [25], it was hypothesized for Eqt II that the coexistence of those phases might be a factor which favors incorporation of the toxin in the monolayer [14].

We then investigated whether the difference in St I binding to monolayers was related to the structural and rheological properties of the lipid model systems. From compression isotherm data of POPC/eSM films we could assign a Le character to all the binary monolayers at 20 mN·m^{-1}, the initial condition selecting for studying St I penetration into monolayers. This conclusion was based on the smooth behavior observed in the compression curves (see Supplementary material, Fig. S1) and the analysis of the compressibility modulus (Cs^{-1}). Table 1 shows that all the POPC/eSM films have low Cs^{-1} (<150 mN·m^{-1}), which fall into the range previously observed for most PC and SM considered to be in the Le state [26,27].

However, even though the above study gives general information about the overall rheology properties of the film, it does not provide any information about the microstructure of the monolayer. Then, we performed BAM visualization of the lipid films at 20 mN·m^{-1}, which revealed that all studied POPC/eSM monolayers exhibited a homogeneous dark gray phase and hence no phase coexistence was observed (not shown). In spite of the generally accepted viewpoint that phase coexistence or domain borders govern the affinity of actinoporins for the membrane [14–17], these results clearly support the idea that these factors are not crucial for binding to membranes, at least in the monolayer system. Other physical properties of the lipid films may be involved in the modulation of St I binding and penetration to PC/SM lipid monolayers.

The lateral diffusion of a lipophilic fluorophore in the POPC/eSM mixtures, was investigated using FRAP experiments. The photobleaching recovery of a selected area of Rho-PE labeled films at 20 mN·m^{-1} was imaged at different times. Representative experiments are shown in Fig. 2A–E and the corresponding FRAP curves in Fig. 2F. As a measure of lipid mobility, the parameter $t_{3/4}$ was calculated, which corresponds to the time required to recover 75% of the initial monolayer fluorescence. $t_{3/4}$ steeply increased with the eSM content in POPC:eSM mixtures (Table 1), showing that a high SM content decreases significantly membrane fluidity, even for films in similar phase states (Le phases). In fact, it should be noticed that for pure eSM monolayer $t_{3/4}$ parameter could not be calculated since the fluorescence was not recovered even after a much longer time (>133 s) (see Fig. 2E).

The scarce affinity of St I for monolayers containing a low amount of SM (≤30 mol%) could be due to the essential role of SM on the interaction of sticholysins with membranes as has been documented for this and other actinoporins [3,8–13]. The increase in SM proportion to 50 mol% prompted an enhanced binding of St I to the monolayers; in fact at this equimolar ratio we observed the highest rate and extent of binding to the membrane (see Fig. 1).

FRAP results reflect the shear viscosity of the lipid film since the lateral movement of a labeled lipid should induce a shear compression over the continuous lipid phase [28]. This phenomenon may also be of importance in the penetration process of a toxin into the lipid
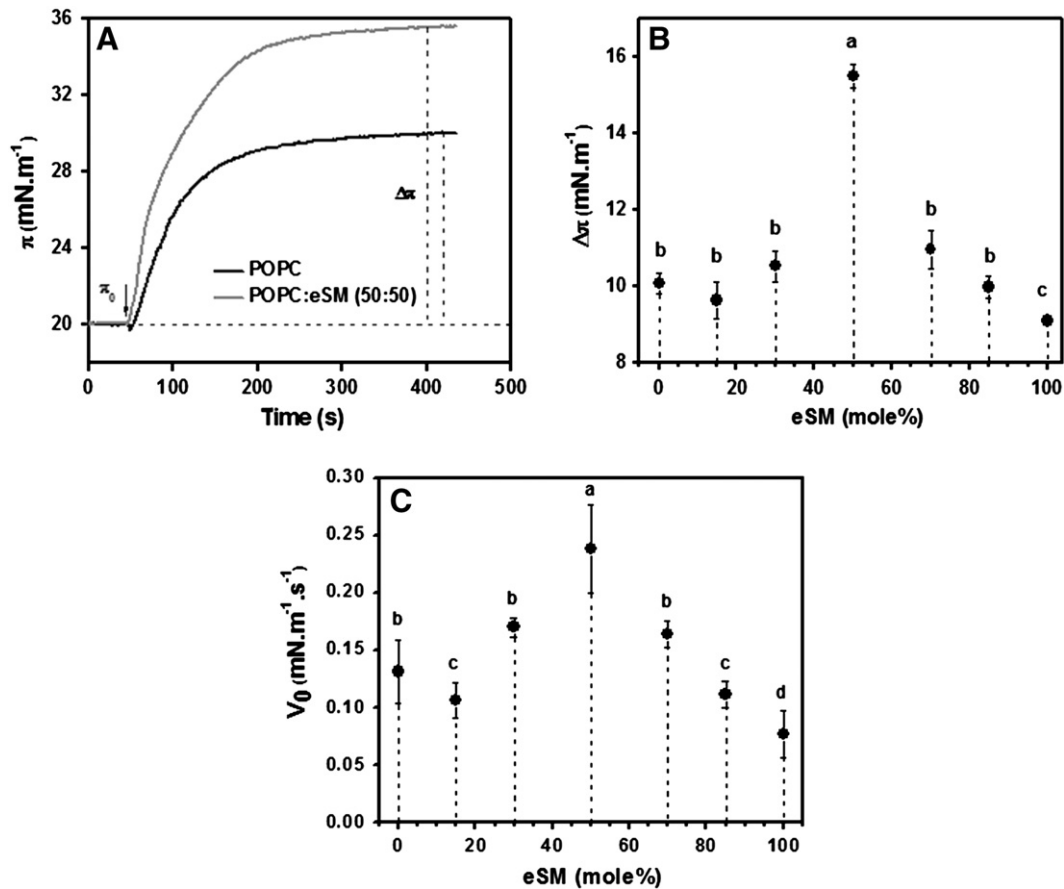
Fig. 1. Interaction of St I with PC/eSM monolayers. (A) Time profile of the increase in π after St I addition. The arrow indicates the time of St I addition. (B) Effect of eSM molar fraction on the St I induced Δπ calculated as the difference between the final π value and π_0. (C) Effect of eSM molar fraction on V_0 of the π increase caused by St I. Experiments were carried out under constant stirring. T: 23 ± 2 °C. St I concentration: 0.8 μM. π_0: 20 mN·m^{-1}. The bars indicate the standard deviation from a set of at least three independent experiments. When no error bar is observed the corresponding standard deviation value is smaller than the size of the symbol. Statistical analysis was performed with one-way ANOVA with Tukey as post-hoc test. The letters a, b, c and d indicate independent groups with significant differences among them ($p < 0.05$).

monolayer since its insertion to the membrane will cause a lateral displacement of lipid components. It has been demonstrated that Eqt II binding to lipid membranes is a two step process: a first binding step followed by a conformational change leading to the irreversible insertion to the membrane of the N-terminal region [7]. This last step appears to involve local displacement and rearrangement of lipid molecules and probably longer range disruption of lipid–lipid interactions. Such processes may be favored by a fluid, easily deformable phase as provided by the Le monolayers with SM content up to 50 mol%. Larger proportions of SM elicit a striking decrease in both the extent and the rate of St I binding, probably associated to a restricted lateral diffusion (and thus, high shear viscosity) of the film, which is proportional to the SM content (Table 1). An extreme situation occurs in monolayers formed

by pure eSM in which a slower lateral diffusion of lipids is observed (Fig. 2 and Table 1). This low fluidity of the lipid film might impair St I insertion into the film. Therefore, fluidity more than phase coexistence appears to be a main regulatory factor for St I binding to PC/SM monolayers.

3.2. Effect of phospholipid acyl chain length and unsaturation on St I interaction with PC/eSM monolayers

To further evaluate the role of the structural and rheological properties of membrane on St I binding to lipid monolayers we proceeded to study the effect of phospholipid acyl chain length and unsaturation. To this end we used PC containing different symmetric saturated acyl chains of 14, 16, 18, and 20C atoms (DMPC, DPPC, DSPC, and DAPC, respectively) and the unsaturated 18:1 acyl chain (DOPC).

St I inserted to a similar extent in PC/eSM monolayers regardless of the type of PC employed, as evidenced by similar values of Δπ at equilibrium (Fig. 3A and Table 2). However, the St I association rate was similar in all the systems containing PC with 14 to 18C fatty acids in contrast to monolayers with DAPC, for which the rate of St I incorporation was significantly lower. The extent and rate of St I association to the unsaturated DOPC containing monolayer did not experience any change when compared to films containing the saturated PC, (DSPC) with the same acyl chain length (Fig. 3B and Table 2).

The structural and rheological properties of the above PC/eSM (50:50) monolayers were also studied by BAM visualization of the compression isotherms. Binary monolayers containing PC with the shortest (DMPC/eSM) or unsaturated acyl chains (DOPC/eSM) showed a Le

Table 1
Characterization of PC/eSM monolayers by compression isotherms and FRAP experiments.

Composition	Cs^{-1} (mN·m^{-1})[I]	$t_{3/4}$ (s)[II]
POPC	75 ± 5	1.2 ± 0.4^d
POPC/eSM (85:15)	80 ± 1	n.d
POPC/eSM (70:30)	79 ± 1	n.d
POPC/eSM (50:50)	86 ± 2	2.4 ± 0.8^c
POPC/eSM (30:70)	90 ± 3	4.2 ± 0.2^b
POPC/eSM (15:85)	79 ± 2	11.6 ± 0.2^a
eSM	79 ± 2	>133

[I] Cs^{-1}: compressibility modulus of lipid monolayers at 20 mN·m^{-1} after Eq. (1).
[II] $t_{3/4}$: time required for recovering 75% of initial fluorescence after bleaching. Mean $\pm$ SEM from two independent experiments are shown. Statistical analysis was performed with one-way ANOVA with Tukey as post-hoc test. The letters a, b, c and d indicate independent groups with significant differences among them ($p < 0.05$). n.d, not determined.
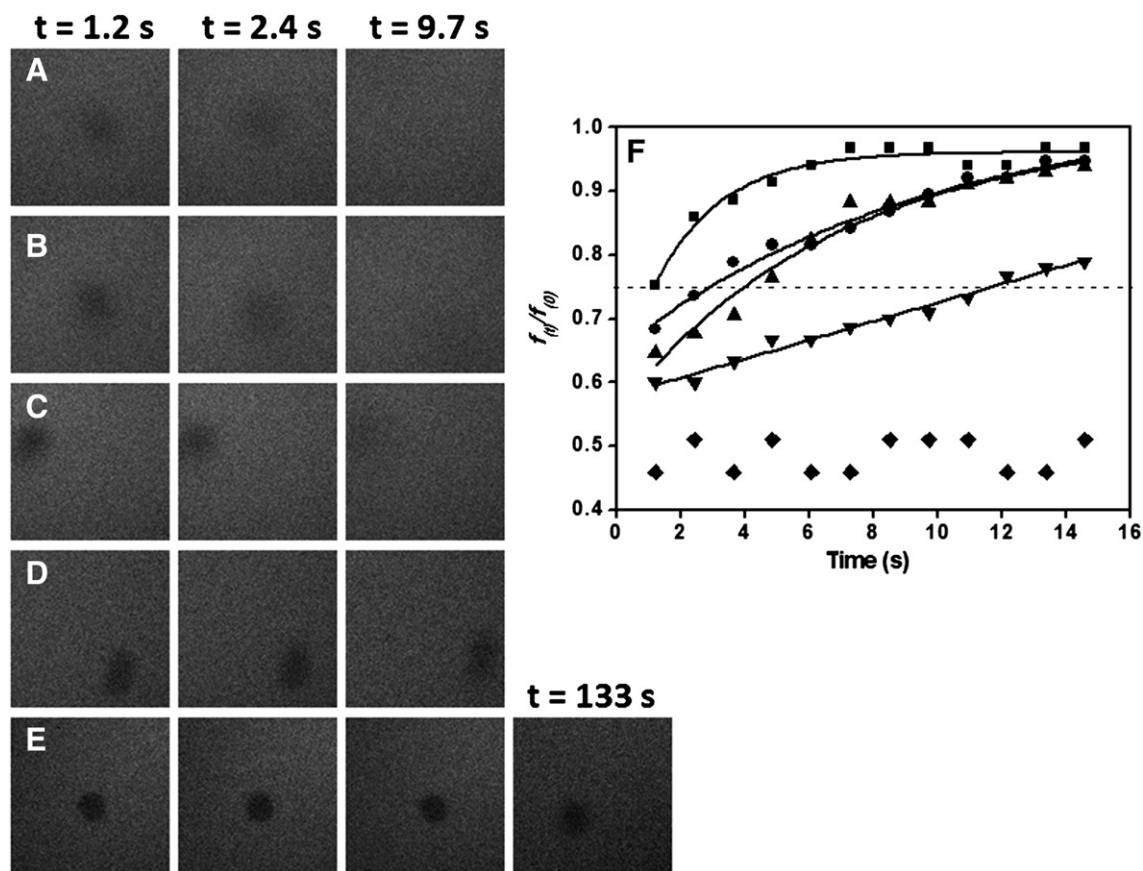
Fig. 2. FRAP characterization of PC/eSM monolayers. Images from temporal series taken during representative FRAP experiments on lipid monolayers. The time after bleaching is indicated in each column. Lipid composition: (A) POPC, (B) POPC/eSM (50:50), (C) POPC/eSM (30:70), (D) POPC/eSM (15:85) and (E) eSM. (F) Normalized fluorescence recovery curves after bleaching a circular area. Full lines represent the best fits of fluorescence recovery data to an exponential function (Eq. (2)). Statistical analysis of these experiments is shown in Table 1. Image size is 100 × 100 μm and bleaching area is 20 μm diameter. Lipid composition: (■) POPC, (●) POPC/eSM (50:50), (▲) POPC/eSM (30:70), (▼) POPC/eSM(15:85) and (♦) eSM. Images are representative of two independent experiments. T: 23 ± 2 °C.

character over the whole pressure range, as evidenced by the monotonic behavior of their compression isotherms, while DPPC/eSM and DSPC/eSM monolayers showed a Le/Lc phase transition starting at ~17 and ~14 mN·m^{-1}, respectively (see Supplementary material, Fig. S2). In contrast, the DAPC/eSM film exhibited a high response in π upon a minimal compression over the whole pressure range, typical of a Lc phase (Fig. S2). All but DAPC/eSM monolayers at 20 mN·m^{-1} showed Cs^{-1} values <150 mN·m^{-1}, as expected for Le phases or Le/Lc transition

region [26,27], while DAPC/eSM monolayers showed Cs^{-1} ~200 mN·m^{-1}, confirming a Lc state (Table 2). It is clear then that the rheological properties of the studied monolayers do not appear to affect the extent of St I incorporation into the film (Δπ). However the reduced rate of St I penetration in the DAPC/eSM monolayer seems to be correlated with the condensed state of this monolayer.

The lateral organization and microstructure of the PC/eSM films at 20 mN·m^{-1} were inspected by BAM. The gray level of BAM images is
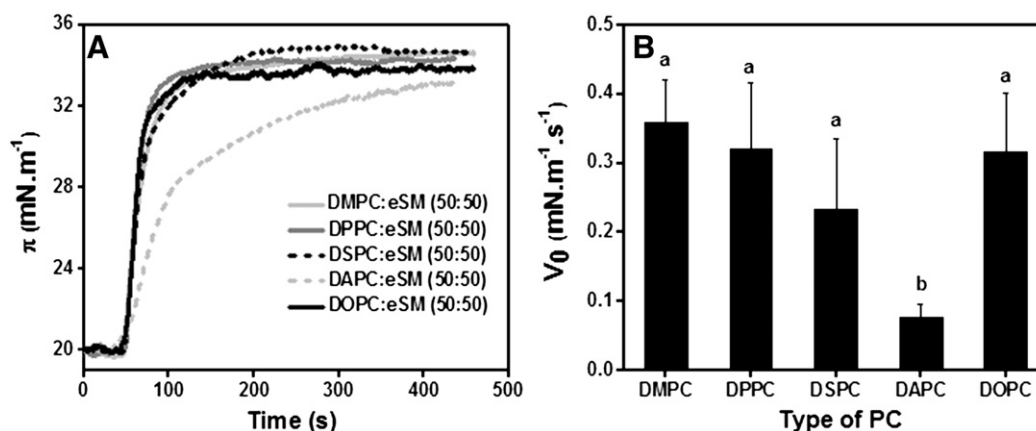
Fig. 3. Effect of PC acyl chain length and unsaturation on the interaction of St I with PC/eSM monolayers. (A) Time profile of the increase in π following St I addition. (B) V_0 of π increase caused by St I insertion into PC/eSM (50:50) monolayers with different types of PC. Experiments were carried out under constant stirring. T: 23 ± 2 °C. π_0: 20 mN·m^{-1}. St I concentration: 0.8 μM. Bars show the mean of V_0 and their standard deviation from at least three independent experiments. Statistical analysis was performed with one-way ANOVA with Tukey as post-hoc test. The letters a, b, c and d indicate independent groups with significant differences among them (p < 0.05).

Table 2
St I penetration into PC/eSM monolayers composed of different PC types.

Composition	$\Delta\pi$ $(mN\cdot m^{-1})^a$	V_0 $(mN\cdot m^{-1}\cdot s^{-1})^b$	Cs^{-1} $(mN\cdot m^{-1})^c$	Phase state
DMPC/eSM	15 ± 1	0.36 ± 0.06	87 ± 1	Le
DPPC/eSM	14 ± 1	0.32 ± 0.09	31 ± 1	Le/Lc
DSPC/eSM	14 ± 1	0.23 ± 0.10	58 ± 6	Le/Lc
DAPC/eSM	14 ± 1	0.08 ± 0.02	205 ± 21	Lc
DOPC/eSM	14 ± 1	0.32 ± 0.08	60 ± 6	Le

[a] $\Delta\pi$: is the π increase of the lipidic monolayer due to St I binding.
[b] V_0: the initial maximal rate of the $\Delta\pi$.
[c] Compressibility modulus of lipid monolayers at 20 mN·m^{-1}. Mean $\pm$ SEM from two independent experiments are shown.

proportional to both the refraction index of the film and the film thickness [29]. Then, Lc domains, which are usually thicker and show higher refraction index, appear as light gray areas surrounded by a dark gray (Le) phase. A uniform dark phase of a Le character was observed in both DMPC/eSM and DOPC/eSM films (Fig. 4A and E), while DPPC/eSM and DSPC/eSM films showed Le/Lc phase coexistence (Fig. 4B and C). On the other hand, DAPC/eSM showed BAM images with higher gray levels (Fig. 4D), which corresponds to a Lc film.

Our results, summarized in Table 2, suggest that the rheological properties of the membrane regulate the velocity of St I penetration process. Thus, a faster incorporation of St I into PC/eSM (50:50) monolayers is observed when a continuous Le phase occurs, independently of the presence of isolated Lc domains when compared with the monolayers showing a Lc phase only.

Even though in all the monolayers studied the final penetration extent of St I accommodation appears to be similar (Fig. 3A and $\Delta\pi$ in Table 2), the consequence of a faster penetration kinetic for the more fluid phases can be relevant in the cellular environment, where several events occur in a far-from-equilibrium situation. For instance the fast and/or transient insertion of the N terminal region of St I may lead to oligomerization steps and pore formation, as described for Eqt II [7], which may be hindered by a less fluid lipid bilayer.

Furthermore St I association to PC/SM (50:50) monolayers is not enhanced by Le/Lc phase coexistence, for instance in DPPC/eSM and DSPC/eSM monolayers, and just the presence of an Le phase is sufficient to increase the rate of St I penetration into the membrane (Table 2).

3.3. St I visualization in transferred monolayers

In order to get further insight into the preferential localization of St I in monolayers with Le/Lc coexisting phases, we labeled St I with the fluorescent probe Alexa Fluor 488 and mixed it with unlabeled St I in a molar proportion of 1:5 (Alexa-labeled St I:unlabeled St I). The mixture retained the hemolytic activity in the nanomolar concentration range and the capacity to insert into lipid monolayers of St I (data not shown). In order to assess lipid segregation by FM, we included 1 mol% of Rho-PE into the lipid mixtures. In the presence of two physically different phases, this probe has a preferential partition into the less

ordered phase, thus probe exclusion was used as a marker for Lc domains. Toxin-loaded monolayers were transferred onto a pre-coated glass support for FM examination.

In agreement with the BAM experiments, DSPC/eSM (50:50) transferred monolayers at 20 mN·m^{-1} showed Le/Lc phase coexistence by FM (Fig. 5A). In this case, the dark areas correspond to Lc domains and the bright areas are indicative of the Rho-PE-enriched Le phase. The component distribution analysis (see Section 2.8) indicated that the Le phase contained a high proportion of eSM and the Lc phase was nearly exclusively formed by DSPC (Table 3). The double labeled films revealed that Alexa-labeled St I was identified in both lipid phases but with a preferential adsorption to the continuous Le phase (Fig. 5D and Table 3). This is an expected result, since the Lc phase was almost devoid of eSM. However, in binary monolayers of SM 18:0/POPC (70:30) or SM18:0/SM18:1 (70:30) at 20 mN·m^{-1}, which also show Le/Lc phase coexistence (Fig. 5B and C, respectively), the double labeled images also showed a slight to moderate preference for the Le phases (Fig. 5E and F), even though the Lc domains showed a higher concentration of SM or both phases were entirely composed of this sphingolipid (Table 3).

Our results show that St I was able to bind to both Le and Lc lipid phases provided SM is present in both phases, but with a general preferential adsorption to Le phases. In the SM 18:0/POPC (70:30) monolayer, St I encounters two opposite phase targets: an Lc phase, exclusively formed by the saturated SM and an Le phase also containing a high amount of SM, but confined to a more fluid state. In this scenario, the toxin is almost unable to distinguish between both phases probably because they have different but equally attractive properties for an optimal St I binding to membrane (Fig. 5E and Table 3).

Furthermore, using a monolayer composed by a mixture of saturated and unsaturated SMs [SM 18:0/SM 18:1 (70:30)] St I partitioned preferentially to the Le phase. This result clearly evidences that the lateral concentration of SM is not the only factor determining the protein binding to monolayer but also the phase state of the target membrane. This finding supports the conclusions drawn in the two previous sections where a high fluid Le phase provides a favorable scenario for St I binding and penetration of lipid monolayers.

It is noteworthy to point out that, differently to equinatoxin II, which has been reported to show a preferential partition in the liquid-ordered domain borders in monolayers [14] and giant unilamellar vesicles [15], we could not observe an enhanced fluorescence at the Lc domain borders in any of the monolayers studied, at least within the detection limit of our experimental approach. This fact discourages assignment of a preferential adsorption of St I to the linear interface between coexisting Lc–Le domains. Furthermore, from our data, we cannot disregard the possibility that this difference could be reflecting that St I and Eqt II, although being members of the actinoporin protein family, might behave differently during their interaction with membrane interfaces. Another explanation could arise from the fact that the domain boundaries of Lc (this work) or liquid ordered phases studied for Eqt II [14,15] may have different properties that modulate the affinity of actinoporins for both types of interfaces.
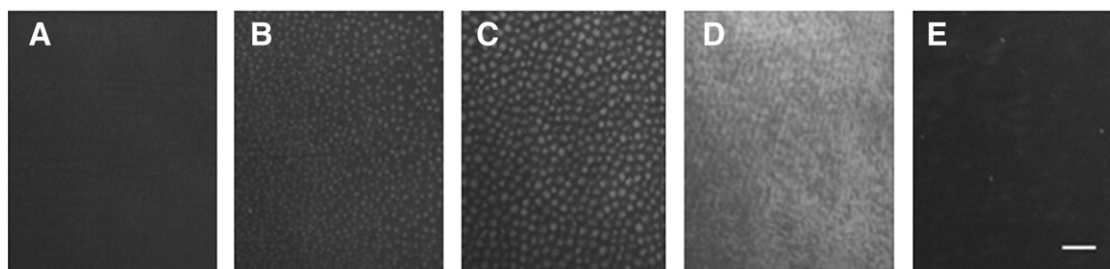
Fig. 4. BAM visualization of PC/eSM (50:50) monolayers of different PC types. Lipid composition: (A) DMPC/eSM, (B) DPPC/eSM, (C) DSPC/eSM, (D) DAPC/eSM and (E) DOPC/eSM. π0: 20 mN·m^{-1}. For better visualization, the lower 0–90 gray level range (from the 0 to 255 original scale) was selected in order to keep the gray level-film thickness ratio. The insets show the same images enhanced by a bandpass filter. Images are representative of two independent experiments. The scale bar in (E) represents 100 μm. T: 23 $\pm$ 2 °C.
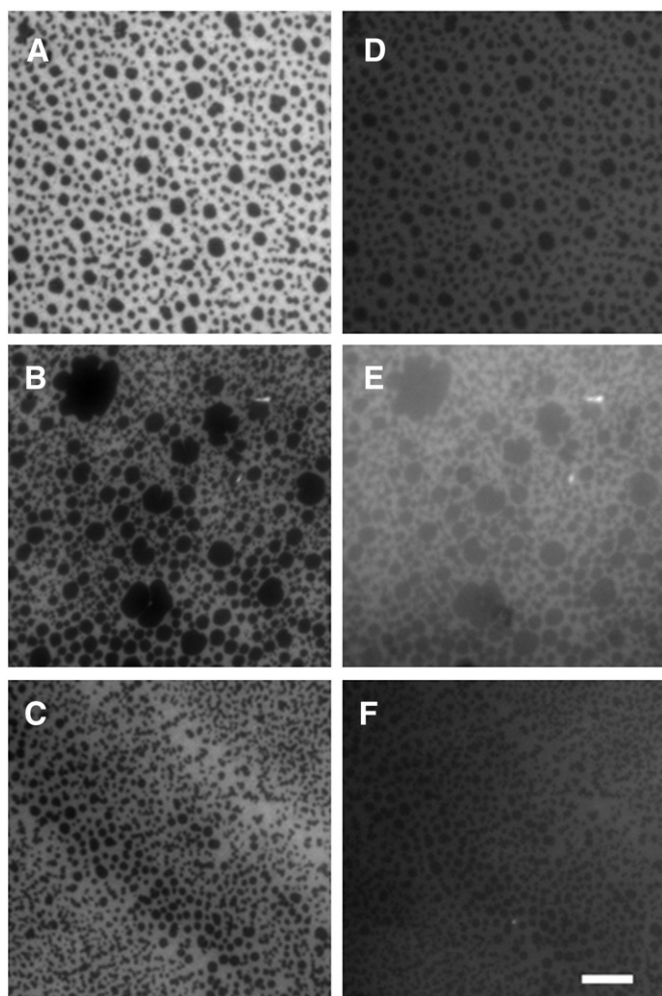
Fig. 5. Epifluorescence microscopy images of St I bound to different monolayers showing coexistence of lipid phases. The left column (A–C) shows the images of different lipid monolayers through a Rhodamine filter and in the right column (D–F) are the same frames imaged through an Alexa 488 filter. Lipid composition: (A) DSPC/eSM (50:50), (B) SM 18:0/POPC (70:30) and (C) SM 18:0/SM 18:1 (70:30) containing in all cases 1 mol% of Rho-PE. π_0: 20 mN·m^{-1}. Alexa 488-labeled St I concentration: 0.8 μM. The scale bar in (F) represents 10 μm. T: 23 ± 2 °C.

regard, the capacity of SM to form both inter- and intramolecular hydrogen bonds may be of importance. It has been previously suggested that hydrogen (H)-bonding between lipids and amphitropic proteins may introduce an important energetic contribution to protein anchoring to membranes [30]. On the other hand, SM bilayers in the liquid disordered phase show a predominance of intramolecular and lipid–water over intermolecular SM–SM H-bonding [31]. This may imply a higher potential for the toxin–SM interaction in the disordered state since it would avoid extensive breaking of stronger SM–SM H-bonding that is established in the gel state.

Other differences between SM and PC membranes that may influence the overall St I binding energetic could be the difference in the hydration (amount of hydration shell and/or water molecule orientation) around the polar head group. SM can closely associate an increased number of water molecules to the phosphocholine group than PC [32, 33]. Thus, preferential binding of the toxin to SM-rich regions in the fluid state would lead to an entropically favored larger release of intermolecular water compared to binding to PC membranes.

4. Conclusions

The results obtained in this investigation support the notion that binding of St I to membranes results from an interplay between the presence of SM and membrane fluidity, with negligible influence of the presence of domain boundaries. Once the membrane has a high availability of SM (>30 mol%) its phase state and rheological properties acquire a major role for the recognition and binding steps of the mechanism of action of sticholysins. We have provided direct experimental evidence that a Le phase supports a larger binding and faster toxin penetration than a Lc phase and that a high lateral mobility of membrane components is also relevant for this process. Hence, we hypothesize that more fluid phases characterized by weaker lipid cohesion and high toxin–SM H-bonding potentiality provide a suitable environment for St I binding and penetration to the membrane.

Supplementary data to this article can be found online at http://dx.doi.org/10.1016/j.bbamem.2014.03.011.

References

[1] R. Aroian, F.G. van der Goot, Pore-forming toxins and cellular non-immune defenses (CNIDs), Curr. Opin. Microbiol. 10 (2007) 57–61.
[2] G. Anderluh, P. Macek, Cytolytic peptide and protein toxins from sea anemones (Anthozoa: Actiniaria), Toxicon 40 (2002) 111–124.
[3] M. Tejuca, M.D. Serra, M. Ferreras, M.E. Lanio, G. Menestrina, Mechanism of membrane permeabilization by sticholysin I, a cytolysin isolated from the venom of the sea anemone *Stichodactyla helianthus*, Biochemistry 35 (1996) 14947–14957.

Anyway, an open question still remains regarding the properties that SM introduces in membranes differently to PC, that may promote St I binding to membrane. This is an intriguing question since both lipids contain the same phosphocholine head group facing the aqueous interface. Therefore, some energetic contributions to the binding process must be taken into account. Spontaneous partitioning of the toxin to the monolayer interface should itself imply a loss of entropy, which could be counteracted by either favorable protein–lipid enthalpic contributions or by entropically favored release of interfacial water. In this

Table 3
St I partition into lipid phases.

Total composition	SM content in the Le phase [a]	SM content in the Lc phase [a]	Le/Lc St I partition ratio[b]
DSPC/eSM (50:50)	84 ± 2	~0	1.29 ± 0.07
SM 18:0/POPC (70:30)	58 ± 2	100 ± 10	1.07 ± 0.02
SM 18:0/SM 18:1 (70:30)	100	100	1.18 ± 0.04

[a] Values that stand for the proportion (%) of the particular lipid of the total lipidic molecules in that phase were calculated after Eq. (3).
[b] The partition ratio was calculated from the gray level measurement of different phases of each picture. Mean ± SEM from at least ten measures accomplished in two independent experiments are shown.

[4] J.M. Mancheño, J. Martín-Benito, M. Martínez-Ripoll, J.G. Gavilanes, J.A. Hermoso, Crystal and electron microscopy structures of sticholysin II actinoporin reveal insights into the mechanism of membrane pore formation, Structure 11 (2003) 1319–1328.

[5] A.E. Mechaly, A. Bellomio, D. Gil-Carton, K. Morante, M. Valle, J.M. González-Mañas, D.M. Guerin, Structural insights into the oligomerization and architecture of eukaryotic membrane pore-forming toxins, Structure 19 (2011) 181–191.

[6] M.E. Lanio, V. Morera, C. Álvarez, M. Tejuca, T. Gómez, F. Pazos, V. Besada, D. Martínez, V. Huerta, G. Padrón, C.M. de los Angeles, Purification and characterization of two hemolysins from *Stichodactyla helianthus*, Toxicon 39 (2001) 187–194.

[7] Q. Hong, I. Gutiérrez-Aguirre, A. Barlic, P. Malovrh, K. Kristan, Z. Podlesek, P. Macek, D. Turk, J.M. González-Mañas, J.H. Lakey, G. Anderluh, Two-step membrane binding by Equinatoxin II, a pore-forming toxin from the sea anemone, involves an exposed aromatic cluster and a flexible helix, J. Biol. Chem. 277 (2002) 41916–41924.

[8] B. Bakrac, I. Gutiérrez-Aguirre, Z. Podlesek, A.F. Sonnen, R.J. Gilbert, P. Macek, J.H. Lakey, G. Anderluh, Molecular determinants of sphingomyelin specificity of a eukaryotic pore-forming toxin, J. Biol. Chem. 283 (2008) 18665–18677.

[9] A.W. Bernheimer, L.S. Avigad, Properties of a toxin from the sea anemone *Stoichacis helianthus*, including specific binding to sphingomyelin, Proc. Natl. Acad. Sci. U. S. A. 73 (1976) 467–471.

[10] V. De los Ríos, J.M. Mancheño, M.E. Lanio, M. Oñaderra, J.G. Gavilanes, Mechanism of the leakage induced on lipid model membranes by the hemolytic protein sticholysin II from the sea anemone *Stichodactyla helianthus*, Eur. J. Biochem. 252 (1998) 284–289.

[11] B.B. Bonev, Y.H. Lam, G. Anderluh, A. Watts, R.S. Norton, F. Separovic, Effects of the eukaryotic pore-forming cytolysin Equinatoxin II on lipid membranes and the role of sphingomyelin, Biophys. J. 84 (2003) 2382–2392.

[12] A. Drechsler, G. Anderluh, R.S. Norton, F. Separovic, Solid-state NMR study of membrane interactions of the pore-forming cytolysin, equinatoxin II, Biochim. Biophys. Acta 1798 (2010) 244–251.

[13] A. Bellomio, K. Morante, A. Barlic, I. Gutiérrez-Aguirre, A.R. Viguera, J.M. González-Mañas, Purification, cloning and characterization of fragaceatoxin C, a novel actinoporin from the sea anemone *Actinia fragacea*, Toxicon 54 (2009) 869–880.

[14] A. Barlic, I. Gutiérrez-Aguirre, J.M. Caaveiro, A. Cruz, M.B. Ruiz-Argüello, J. Pérez-Gil, J.M. González-Mañas, Lipid phase coexistence favors membrane insertion of equinatoxin-II, a pore-forming toxin from *Actinia equina*, J. Biol. Chem. 279 (2004) 34209–34216.

[15] P. Schon, A.J. García-Saez, P. Malovrh, K. Bacia, G. Anderluh, P. Schwille, Equinatoxin II permeabilizing activity depends on the presence of sphingomyelin and lipid phase coexistence, Biophys. J. 95 (2008) 691–698.

[16] J. Alegre-Cebollada, I. Rodríguez-Crespo, J.G. Gavilanes, A.M. del Pozo, Detergent-resistant membranes are platforms for actinoporin pore-forming activity on intact cells, FEBS J. 273 (2006) 863–871.

[17] D. Martínez, A. Otero, C. Álvarez, F. Pazos, M. Tejuca, M.E. Lanio, I. Gutiérrez-Aguirre, A. Barlic, I. Iloro, J.L. Arrondo, J.M. González-Mañas, E. Lissi, Effect of sphingomyelin and cholesterol on the interaction of St II with lipidic interfaces, Toxicon 49 (2007) 68–81.

[18] I.D. Bianco, B. Maggio, Interactions of neutral and anionic glycosphingolipids with dilauroylphosphatidylcholine and dilauroylphosphatidic acid in mixed monolayers, Colloids Surf. 40 (1989) 249–260.

[19] H.L. Brockman, C.M. Jones, C.J. Schwebke, J.M. Smaby, D.E. Jarvis, Application of microcomputer-controlled film balance system to collection and analysis of data from mixed monolayers, J. Colloid Interface Sci. 78 (1980) 502–512.

[20] D. Martínez, A.M. Campos, F. Pazos, C. Álvarez, M.E. Lanio, F. Casallanovo, S. Schreier, R.K. Salinas, C. Vergara, E. Lissi, Properties of St I and St II, two isotoxins isolated from *Stichodactyla helianthus*: a comparison, Toxicon 39 (2001) 1547–1560.

[21] L. De Tullio, B. Maggio, M.L. Fanani, Sphingomyelinase acts by an area-activated mechanism on the liquid-expanded phase of sphingomyelin monolayers, J. Lipid Res. 49 (2008) 2347–2355.

[22] E.C. Ale, B. Maggio, M.L. Fanani, Ordered-disordered domain coexistence in ternary lipid monolayers activates sphingomyelinase by clearing ceramide from the active phase, Biochim. Biophys. Acta 1818 (2012) 2767–2776.

[23] B. Caruso, A. Mangiarotti, N. Wilke, Stiffness of lipid monolayers with phase coexistence, Langmuir 29 (2013) 10807–10816.

[24] R. Maget-Dana, The monolayer technique: a potent tool for studying the interfacial properties of antimicrobial and membrane-lytic peptides and their interactions with lipid membranes, Biochim. Biophys. Acta 1462 (1999) 109–140.

[25] R.F. de Almeida, A. Fedorov, M. Prieto, Sphingomyelin/phosphatidylcholine/cholesterol phase diagram: boundaries and composition of lipid rafts, Biophys. J. 85 (2003) 2406–2416.

[26] J.M. Smaby, V.S. Kulkarni, M. Momsen, R.E. Brown, The interfacial elastic packing interactions of galactosylceramides, sphingomyelins, and phosphatidylcholines, Biophys. J. 70 (1996) 868–877.

[27] X.M. Li, J.M. Smaby, M.M. Momsen, H.L. Brockman, R.E. Brown, Sphingomyelin interfacial behavior: the impact of changing acyl chain composition, Biophys. J. 78 (2000) 1921–1931.

[28] N. Wilke, M.F. Vega, B. Maggio, Rheological properties of a two phase lipid monolayer at the air/water interface: effect of the composition of the mixture, Langmuir 26 (13) (2010) 11050–11059.

[29] M.L. Fanani, B. Maggio, Liquid-liquid domain miscibility driven by composition and domain thickness mismatch in ternary lipid monolayers, J. Phys. Chem. B 115 (2011) 41–49.

[30] P.K. Kinnunen, A. Koiv, J.Y.A. Lehtonen, M. Rytomaa, P. Mustonen, Lipid dynamic and peripheral interactions of proteins with membranes surfaces, Chem. Phys. Lipids 73 (1994) 181–207.

[31] P. Niemela, M.T. Hyvonen, I. Vattulainen, Structure and dynamics of sphingomyelin bilayer: insight gained through systematic comparison to phosphatidylcholine, Biophys. J. 87 (2004) 2976–2989.

[32] G.G. Shipley, L.S. Avecilla, D.M. Small, Phase behavior and structure of aqueous dispersions of sphingomyelin, J. Lipid Res. 15 (1974) 124–131.

[33] D. Bach, I.R. Miller, Hydration of phospholipid bilayers in the presence and absence of cholesterol, Chem. Phys. Lipids 136 (2005) 67–72.